Applied Catalysis B: Environmental 152–153 (2014) 99–107

Contents lists available at ScienceDirect

Applied Catalysis B: Environmental

journal homepage: www.elsevier.com/locate/apcatb

Preparation, characterisation and testing of $CuO/Ce_{0.8}Zr_{0.2}O_2$ catalysts for NO oxidation to NO_2 and mild temperature diesel soot combustion

Javier Giménez-Mañogil, Agustín Bueno-López, Avelina García-García*

MCMA Group, Department of Inorganic Chemistry, Faculty of Sciences, University of Alicante, Ap.99-E-03080 Alicante, Spain

ARTICLE INFO

Article history:
Received 12 November 2013
Received in revised form
30 December 2013
Accepted 10 January 2014
Available online 22 January 2014

Keywords:
Copper content
$NO_x + O_2$
$Ce_{0.8}Zr_{0.2}O_2$
NO oxidation to NO_2
Diesel soot combustion.

ABSTRACT

CuO/ceria-zirconia catalysts have been prepared, deeply characterised (N_2 adsorption–desorption isotherms at −196 °C, XRD, Raman spectroscopy, XPS, TEM and H_2-TPR) and tested for NO oxidation to NO_2 in TPR conditions, and for soot combustion at mild temperature (400 °C) in a NO_x/O_2 stream. The behaviour has been compared to that of a reference Pt/alumina commercial catalyst. The ceria-zirconia support was prepared by the co-precipitation method, and different amounts of copper (0.5, 1, 2, 4 and 6 wt%) were loaded by incipient wetness impregnation.

The results revealed that copper is well-dispersed onto the ceria-zirconia support for the catalysts with low copper loading and CuO particles were only identified by XRD in samples with 4 and 6% of copper. A very low loading of copper increases significantly the activity for the NO oxidation to NO_2 with regard to the ceria-zirconia support and an optimum was found for a 4% CuO/ceria-zirconia composition, showing a very high activity (54% at 348 °C). The soot combustion rate at 400 °C obtained with the 2% CuO/ceria-zirconia catalyst is slightly lower to that of 1% Pt/alumina in terms of mass of catalyst but higher in terms of price of catalyst.

1. Introduction

Cerium-based oxides have been studied in the framework of heterogeneous catalysis in recent years, and they have been used to control emissions of pollutants from the exhaust gases of gasoline engines in the three-way catalysts (TWCs). The key to understand the operation of these materials on TWC is based on their ability to release and store oxygen due to the redox couple Ce^{3+}/Ce^{4+}. The facility with which these catalysts improve oxygen mobility in the lattice is enhanced by the inclusion of other cations forming substitutional solid solutions, which can lead to non-stoichiometric mixed oxides. The final properties of these compounds depend on the conditions of temperature and gas atmosphere in which they are located. One of the most commonly used mixed oxides is ceria-zirconia ($Ce_xZr_{1-x}O_2$). Zirconium replaces cerium in their crystal lattice positions. This distorts the characteristic cubic fluorite structure of ceria and promotes the creation of oxygen vacancies, thereby facilitating the cerium oxide redox properties and the oxygen mobility in the lattice. Zirconium doping confers thermal stability to ceria as well. The importance of these mixed oxides as catalysts has raised several studies for application to different oxidation reactions [1–7].

Catalysts based on noble metals, such as platinum, have been developed to promote the oxidation of NO to NO_2, which is more oxidant than O_2, and decrease the combustion onset temperature of soot. However, their high cost has led to the study of other lower-priced materials that can be competitive in terms of catalytic activity. These include, besides cerium-based catalysts, those using transition metals. The use of supported or exchanged copper into a cerium-based oxide improves the catalytic properties, as several studies indicate [8–13].

Copper-doped ceria (ceria-zirconia) mixed oxides have managed to overcome activity and selectivity of undoped oxides in reactions such as soot combustion [14,15]. As reported in the literature, copper-based catalysts have been investigated for the NO oxidation to NO_2 as well, using different supports, such as: zeolites [16–18], alumina, titania, perovskites [19–21], and also ceria [9,14,22]. In general terms, these studies point out that the copper-based catalysts enhance the activity towards the NO oxidation to NO_2, even at low temperatures, with regard to the bare supports. Therefore, active catalysts with formulation $CuO/Ce_xZr_{1-x}O_2$ are promising candidates to replace noble metals catalysts, but with lower cost. The ceria-zirconia supports are able to disperse and stabilise copper particles on its surface improving the activity and preventing sintering. The Cu–ceria interface interactions confer a synergistic effect, which enhances the redox properties of the catalyst due to the stabilisation of highly reactive copper species [8–13,21,23–25]. These types of catalysts have already been studied in other reactions with technological interest, such

* Corresponding author. Tel.: +34 965909419; fax: +34 96590 3454.
E-mail address: a.garcia@ua.es (A. García-García).

0926-3373/$ – see front matter © 2014 Elsevier B.V. All rights reserved.
http://dx.doi.org/10.1016/j.apcatb.2014.01.018

as CO oxidation, CO preferential oxidation in H_2-rich streams (CO-PROX) or methanol synthesis from CO and H_2 [8,12,13,26–30].

The overall aim of this research is the preparation and detailed characterisation of mixed oxides with $CuO/Ce_{0.8}Zr_{0.2}O_2$ formulation, prepared with several copper contents, and its application to the catalytic NO oxidation to NO_2 and soot combustion in a NO_x/O_2 gas mixture. The choice of the particular formulation $Ce_{0.8}Zr_{0.2}O_2$ for the support has been done according to our previous optimisation studies [2].

2. Experimental

2.1. Catalyst preparation

The $Ce_{0.8}Zr_{0.2}O_2$ mixed oxide (denoted as CZ) has been synthesised by the co-precipitation method in alkaline medium, by using the cerium and zirconium precursors $(NH_4)_2Ce(NO_3)_6$ (supplied by Panreac with 99.0% purity) and $ZrO(NO_3)_2{\cdot}xH_2O$ (supplied by Sigma–Aldrich, with $x \approx 6$, technical grade), respectively. The appropriate amounts of these precursors were dissolved in distilled water. The corresponding hydroxides of cerium and zirconium were co-precipitated by drop wise addition of a 10% ammonia solution in water until pH = 9, under constant stirring. The solid obtained was then filtered under vacuum and the yellowish precipitate was washed with distilled water until neutral pH. Finally it was dried overnight at 110 °C and calcined in air in a muffle at 500 °C for 1 h, with a heating rate of 10 °C/min.

$Ce_{0.8}Zr_{0.2}O_2$-supported copper catalysts with Cu wt% of 0.5, 1, 2, 4 and 6 (denoted as Cu 0.5%, Cu 1%, Cu 2%, Cu 4% and Cu 6%, respectively) were prepared by incipient wetness impregnation with $Cu(NO_3)_2{\cdot}3H_2O$ (supplied by Panreac with 99.0% purity) solutions of different concentration. After impregnation, the samples were dried overnight in an oven at 110 °C and thereafter calcined under air at 500 °C for 1 h, with a heating rate of 10 °C/min. Due to the limitations of the $Cu(NO_3)_2{\cdot}3H_2O$ solubility in water, the Cu 0.5%, Cu 1% and Cu 2% catalysts were impregnated in a single step, while Cu 4% and Cu 6% were prepared by successive impregnations with the solution used to prepare Cu 2%.

In order to verify the reproducibility of the copper impregnation method, the synthesis was repeated in a new batch for Cu 2%. This sample was denoted as Cu 2%-re.

The actual copper content on the catalysts were close to the nominal values, as verified by ICP-OES (Perkin Elmer, Optima 3000). The copper was extracted from the catalysts using a mixture of concentrated HCl/HNO_3 (3/1 ratio).

2.2. Characterisation techniques

The specific surface areas of the samples were determined by the BET method. N_2 adsorption–desorption isotherms were obtained at −196 °C in an automatic volumetric system (Autosorb-6B from Quantachrome) after degassing the samples at 250 °C for 4 h. The specific pore volume was calculated from the desorption branches of the isotherms at $P/P_0 = 0.98$ following the criteria used by Moretti et al. [31]. The pore size distribution of the materials was analysed using the Barrett–Joyner–Halenda (BJH) method.

Powder XRD patterns were recorded in a Bruker D8 advance diffractometer, using the CuKα radiation (λ = 0.15418 nm). Diffractograms were recorded between 10° and 60° (2θ) with a step size of 0.05° and measuring for 3 s at each step. Indexation and calculation of unit cell parameters were performed by using the positions of line (1 1 1) and Bragg's law, considering cubic system for ceria fluorite structure. The estimation of crystal size was carried out using the Scherrer's equation and, due to possible effects of strain in the crystallites; the Williamson–Hall's method was applied as well [32–34]. In order to improve accuracy, crystal sizes were estimated as an average value from those obtained from three representative fluorite reflections ((1 1 1), (2 2 0) and (3 1 1)), since the corresponding individual measurements showed small deviation among each other.

Raman spectra were performed in a Bruker RFS 100/S Fourier Transform Raman Spectrometer with a variable power Nd:YAG laser source (1064 nm). 64 scans at 85 mW laser power (70 mW on the sample) were recorded and no heating of the sample was observed under these conditions.

The TEM analysis was conducted using a JEM-2010 Transmission Electron Microscope (JEOL). The microscope is equipped with an imaging camera SC600 ORIUS (GATAN) which is integrated within the programme of acquisition and image processing.

XPS spectra were obtained using a K-Alpha spectrophotometer (Thermo-Scientific), with a high resolution monochromator. It comprises a source of electrons and ions for automated load compensation. The X-ray radiation source comprises an Al anode (1486.6 eV). The pressure of the analysis chamber was kept at 5×10^{-9} mbar and was kept working with the detector in constant energy mode with pass energy of 200 eV for the survey spectrum and 50 eV for the sweep in each individual region. The binding energy was adjusted using the C 1s transition, appearing at 284.6 eV. Binding energy values measured are accurate to ±0.2 eV. The values of binding energy and kinetic energy were adjusted with the Peak-Fit software of the spectrophotometer.

The Zr 3d, Ce 3d, Ce 4d, Cu 2p and Cu-L_3VV regions were used in order to determine the surface composition of the studied catalysts. The proportion of Ce^{3+} cations with regard to the total cerium on surface was calculated as described by Laachir et al. [35].

The analysis of the Cu-$2p_{3/2}$ and Cu-L_3VV Auger spectra was used to obtain information about the nature of the copper species present on the surface of the samples. The photo reduction of highly dispersed copper species on catalysts due to the irradiation of X-rays in the analysis chamber is possible according to literature [10,36]. In order to compare the results, a sample of CuO has also been analysed. This sample was obtained by calcination of $Cu(NO_3)_2{\cdot}3H_2O$ in the same conditions than those used for the catalysts preparation.

The reducibility of the fresh samples was examined by H_2-temperature programmed reduction (H_2-TPR) in a Micromeritics Pulse ChemiSorb 2705 device consisting of a tubular quartz reactor coupled to a TCD detector in order to monitor H_2 consumption. 20 mg of sample were placed in the reactor for each experiment. The reducing gas used was 5% H_2 in Ar, with a flow rate of 35 ml/min. The temperature range explored was from room temperature to 1000 °C with a heating rate of 10 °C/min. An in situ pre-treatment was carried out under 5% O_2 in He. The sample was heated at 10 °C/min from room temperature up to 500 °C, maintaining the maximum temperature for 60 min.

2.3. Catalytic measurements

The catalytic tests were performed in a tubular quartz reactor coupled to specific NDIR–UV gas analysers (Fisher–Rosemount, models BINOS 100, 1004 and 1001) for CO, CO_2, NO, NO_2 and O_2 monitoring. For the NO oxidation tests, 80 mg of catalyst were diluted with 320 mg of SiC to avoid pressure drop. The gas mixture used comprised 500 ppm NO_x, 5% O_2 and balance N_2; the gas flow was fixed at 500 ml/min >(GHSV = 30,000 h^{-1}). The experimental set-up has been designed in order to ensure that the proportion of NO_2 in the $NO + O_2$ mixture fed to the reactor is negligible. The catalytic tests consisted of temperature programmed reactions, where the temperature was increased from room temperature up to 700 °C at 10 °C/min under the reactive atmosphere, with the

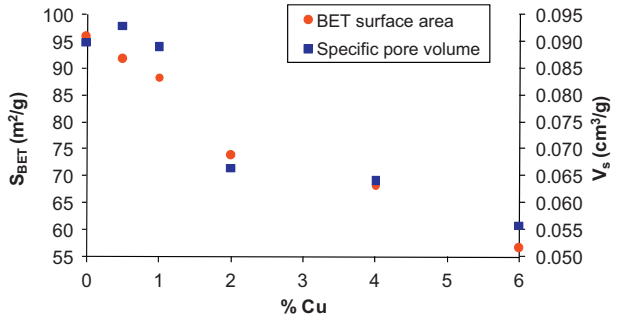

Fig. 1. BET surface areas (in circles) and specific pore volumes (in squares) of the samples versus copper contents.

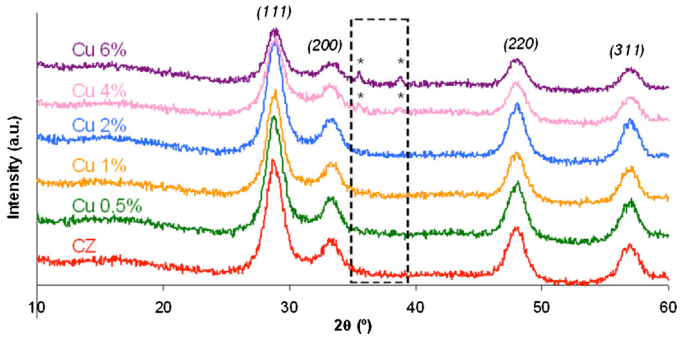

Fig. 2. XRD patterns for the samples (fluorite phase reflections are shown in parentheses, and tenorite phase peaks are marked with *).

purpose of quantifying the NO to NO_2 oxidation capacity of the catalysts.

The NO_2 production profiles were determined in relation to the total amount of NO_x as a temperature function using the following Eq. (1):

$$NO_2(\%) = 100 \times \frac{NO_{2\,output}}{NO_{output}+NO_{2\,output}} \quad (1)$$

where NO_{output} and $NO_{2output}$ are the NO and NO_2 concentrations, respectively, measured at the reactor exit.

Soot combustion tests were performed with selected catalysts in isothermal conditions (400 °C) and with the same gas mixture used for the NO oxidation measurements. 80 mg of catalyst were mixed with 20 mg of soot under loose contact conditions, and diluted with 300 mg of SiC. Temperature programmed reactions, under identical experimental conditions than those used for NO oxidation tests (but with soot) were previously carried out for the selection of the catalysts.

For the sake of comparison, a commercial 1% Pt/Al_2O_3 catalyst, supplied by Sigma–Aldrich with a BET surface area of 160 m^2/g, was also tested in identical conditions than the ceria-zirconia catalysts.

3. Results and discussion

3.1. Textural and structural characterisation

Surface area values (S_{BET}) are shown in Fig. 1 and Table 1. The areas of the copper containing catalysts are lower than that of the parent $Ce_{0.8}Zr_{0.2}O_2$ support (96 m^2/g), and decrease with the copper loading. This trend is in accordance with previous works related to samples prepared by this same procedure [27]. The presence of mesoporosity was assessed from the N_2 physisorption isotherms and the BJH pore size distributions (see Fig. S1a and b from the Supplementary Information).

The specific pore volume (V_s), calculated from the isotherms as described for this kind of materials [31], concurrently diminishes for catalysts with more than 1% copper loading (Fig. 1). These results indicate a certain $Ce_{0.8}Zr_{0.2}O_2$'s pores blocking upon copper incorporation on its surface.

Fig. 2 displays the X-ray diffractograms of the catalysts. Diffraction peaks attributable to cubic fluorite phase of ceria are observed in all cases. Two very weak peaks, characteristic of a CuO phase (tenorite), were also detected at 35.5° and 38.8° for the samples with the highest copper amounts (4% and 6%), indicating that bulk CuO crystallites are formed on these catalysts.

The symmetrical peaks of $Ce_{0.8}Zr_{0.2}O_2$ suggested formation of single ceria-zirconia solid solution (peak splitting would be expected if two phases were segregated). Table 1 lists lattice constants and average crystal sizes. The lattice parameter obtained for pure ceria prepared under identical conditions yielded a value of 0.5406 nm [3], and the lattice constant of $Ce_{0.8}Zr_{0.2}O_2$ (0.5362 nm) is quite congruent with lattice contraction due to zirconium incorporation into the ceria lattice (r_{Ce}^{4+} = 0.097 nm versus r_{Zr}^{4+} = 0.084 nm). Accordingly, the lattice constant obtained for $Ce_{0.8}Zr_{0.2}O_2$ (0.5362 nm) is very close to that determined theoretically by Vegard's law (0.5357 nm) and similar to other literature values reported for a mixed oxide prepared under very similar experimental conditions (0.5370 nm) [5].

As collected in Table 1, lattice parameters estimated for the copper-containing catalysts are close to that of the support. This suggests that copper remains essentially on the surface, and it is not significantly incorporated into the fluorite structure, as could be promoted by other synthesis routes (e.g. micro emulsion–precipitation) [13,27,31].

The XRD patterns also showed very broad main peaks, suggesting, a priori, small crystal sizes. The determination of the crystal sizes can be approached by means of Scherrer's equation in agreement with Zhang et al. [34]. This is accounted for in the supporting information (see Fig. S2 and comments appended).

The mentioned average crystal sizes are also listed in Table 1, revealing that the values obtained for the copper-containing catalysts (in the 5.7–6.4 nm range) remain close to that of the parent ceria-zirconia support (5.5 nm).

The XRD results are well complemented by the Raman study. Fig. 3 shows the Raman spectra of the samples, all with a main band at 473.5 cm^{-1} ascribed to the F_{2g} vibration mode of the fluorite structure of ceria. The intensity of this band decreases by increasing

Table 1
Main parameters obtained from the textural and structural characterisation.

Catalyst	S_{BET} (m^2/g)	Lattice parameter (nm)	Average crystal size (nm)	Phases detected by XRD	F_{2g} band position (cm^{-1})	FWHM[a] (cm^{-1})
CZ	96	0.5362	5.5	Fluorite	473.5	60
Cu 0.5%	92	0.5363	6.1	Fluorite	473.5	57
Cu 1%	88	0.5361	6.4	Fluorite	473.5	62
Cu 2%	71	0.5359	5.9	Fluorite	473.5	62
Cu 4%	68	0.5358	5.7	Fluorite and tenorite	475.5	58
Cu 6%	57	0.5362	5.8	Fluorite and tenorite	473.5	57
Cu 2%-re	74	0.5357	5.9	Fluorite	473.5	65

[a] Full width at half maximum for the F_{2g} Raman peak.

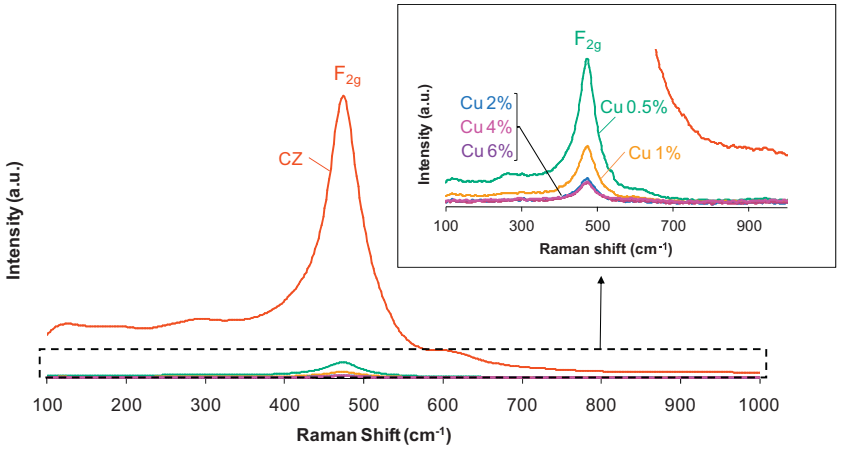

Fig. 3. Raman spectra of the catalysts.

the copper loading, which could be related to the optical absorption of copper. Shan et al. [37] reported much reduced Raman modes for a CuO–CeO_2 physical mixture, compared with pure CeO_2, due to the strong absorption of CuO in the studied region (400–1200 cm^{-1}). However, it must be taken into account that the presence of copper neither affects the position of the F_{2g} band at 473.5 cm^{-1} nor the band broadening (Table 1). Results reveal that copper is not loaded into the ceria-zirconia lattice or there is a small incorporation of copper at surface or subsurface positions of the lattice; which might not be detected by Raman spectroscopy for these catalysts. Copper incorporation into the lattice would have been detected by the red shift and the broadening of the main F_{2g} mode, as published by Gamarra et al. [27].

Finally, very low intensity Raman bands have been found at ≈120 cm^{-1} and 292 cm^{-1} for the ceria-zirconia support spectrum, which can be associated to Zr incorporation into the ceria lattice with the consequent distortion of the framework symmetry. Additionally, the weak and broad band extending between 560 and 650 cm^{-1} can be associated to the presence of oxygen vacancies [26,27,38].

As a conclusion of data obtained by XRD and Raman spectroscopy, it can be predicted the possible existence of the pseudo cubic t'' metastable phase on the ceria-zirconia support [1,3]. This t'' phase differed from the symmetric cubic c phase only in that some oxygen ions are displaced from their ideal octahedral positions of the fluorite structure to new tetragonal positions, while all cations remain in their face cubic centred positions [1,3,29]. This also applies to 0.5% Cu/ceria-zirconia, but is not so obvious for catalysts with higher copper loadings. The progressive loss in Raman intensity with the copper content makes it difficult to distinguish between the t'' and c phases. Finally, the presence of a very weak band detected at 294 cm^{-1} (not apparent due to the scale) for the highest copper-containing sample (Cu 6%) is compatible with the presence of crystalline CuO on this sample, as observed by XRD. This also agrees with previous results from Gamarra et al. [27] where the same minor detectable signal was seen for a 5% Cu/CeO_2 sample.

TEM has been used in order to analyse the morphology of the samples. Fig. S3, from Supplementary Information, illustrates the images of some representative samples: the ceria-zirconia support and the catalysts with 0.5%, 4% and 6% of copper loading. The presence of aggregates of multiple nanoparticles can be generally observed. The interplanar distances of the lattice fringes observed are compatible with the fluorite structure in all cases. Evidences of copper were not found in any of the multiple pictures taken from these samples, in spite of the relatively high copper loading in some of the samples studied [27].

3.2. XPS characterisation

The catalysts were analysed by XPS to verify, semi-quantitatively, the surface composition and the oxidation states of copper [39] and cerium. Table 2 lists the several atomic surface ratios and the Ce^{3+} percentage (with regard to total cerium) on surface. To begin with, the Ce/Zr surface atomic ratios for these samples indicate zirconium enrichment on the periphery of the particles, in accordance with the values of the solubility constants (4×10^{-51} for the cerium (IV) hydroxide, and 2×10^{-48} for the zirconium hydroxide), as explained in a previous article [3]. This ratio is kept more or less constant for all catalysts (see Table 2). The Ce4d/Ce3d ratios provide information about the distribution of cerium in terms of the analysis depth. Higher analysis depth is obtained for Ce4d as a consequence of lower binding energies for this photo-ionisation level. The Ce4d/Ce3d ratios are always higher than 1, which is consistent with the zirconium enrichment on the surface, that is, the cerium concentration increases from the periphery to the subsequent layers of the particles.

The $Cu/(Ce+Zr)_{sur}$ surface ratios were estimated and compared to the bulk atomic ratios (appearing as $Cu/(Ce+Zr)_{nom}$ in Table 2). The ratio between these two parameters ($Cu/(Ce+Zr)_{sur}$ divided between $Cu/(Ce+Zr)_{nom}$) is a measurement of the copper enrichment on surface. All the samples present a copper-rich surface, as expected, and this enrichment increases linearly with the copper content from 1.19 to 3.85 (representation illustrated on Fig. S4 of the Supporting Information). This means a very good distribution of copper inside the accessible porosity, mainly for the catalysts with lower amount of copper, as the copper enrichment is close to 1; even though some copper substitution on the surface level could not be discarded. While an excess of copper remains essentially as CuO_x entities on the surface, exceeding the capacity of support dispersion. Accordingly, small CuO segregated crystallites have been identified by XRD for the Cu 4% and Cu 6% samples.

The identification of the Ce oxidation state on the samples was performed as reported in the literature [35]. The chemical valence of cerium on surface of the catalysts was mainly in a +4 oxidation state, as expected. There are no significant differences in the samples, and all the values range between 29 and 35% of Ce^{3+}. These high values cannot be ascribed solely to the presence of a cerium reduced state associated to the existence of oxygen vacancies, but also to the presence of $Ce_2CO_3 \cdot xH_2O$, as proved by high carbon contents on the elemental atomic analysis. This is consistent with $O/(Cu+Ce+Zr)$ values higher than 2 for all the samples analysed. Moreover, the spontaneous reduction that ceria-zirconia materials could suffer by the action of the X-ray irradiation combined with

Table 2
Surface atomic ratios estimated by XPS.

	Ce3d/Zr3d[a]	Ce4d/Ce3d	$Cu/(Ce+Zr)_{sur}$	$Cu/(Ce+Zr)_{nom}$	Cu Enrichment[b]	Ce^{3+} (%)	$O/(Cu+Ce+Zr)$
CZ	2.5	1.1	–	–	–	35.8	2.5
Cu 0.5%	2.3	1.2	0.015	0.013	1.19	35.7	2.4
Cu 1%	2.6	1.1	0.037	0.026	1.46	33.0	2.3
Cu 2%	2.0	1.3	0.095	0.051	1.85	34.3	2.4
Cu 4%	2.4	1.3	0.282	0.102	2.76	31.5	2.1
Cu 6%	2.1	1.1	0.590	0.153	3.85	28.8	2.1
Cu 2%-re	2.4	1.1	0.100	0.051	1.97	31.4	2.3

[a] The nominal value of Ce/Zr is 4.
[b] The Cu enrichment is defined as the ratio between $Cu/(Ce+Zr)_{sur}$ and $Cu/(Ce+Zr)_{nom}$.

ultra-high-vacuum environment should not be discarded. All these issues were well commented in a previous publication [40].

Regarding the analysis of the surface copper, Cu-2p photoelectron and Cu-L_3VV Auger spectra have been rigorously analysed in an attempt to obtain information about the nature of the copper species. Usually, the characterisation of the oxidation states of copper is performed by comparing the Cu-$2p_{3/2}$ peak position and Auger parameter values (α') in a Wagner plot [41]. However, an extensive review of the literature data points out the intrinsic difficulty in the identification of the copper oxidation state on an XPS-only basis, particularly in cases where the copper phase is highly dispersed onto a support [10,42–44]. In this sense, Espinós et al. [39] proved that this procedure may result in misleading data, because both parameters (Cu-$2p_{3/2}$ peak position and Auger parameter) showed to be affected by the degree of copper dispersion in a series of CuO samples supported on various oxides, such as ZrO_2.

Therefore, the evolution of Auger Cu-L_3VV and Cu-$2p_{3/2}$ spectra for copper catalysts are shown in Figs. 4 and 5 respectively. For comparative purposes, the profile obtained with a CuO bulk reference sample has been included in the representations. The position of the main peak shifts to higher kinetic energies with the copper content in the Auger spectra series (Fig. 4) and higher binding energy values of the Cu-$2p_{3/2}$ peak position (Fig. 5) are found as well. All these data are shown in Table 3, revealing that they are very sensitive to the copper dispersion degree on the support, according to Espinós et al. [39]. Additionally, Table 4 shows the representative values of binding energy and Auger parameter, taken from the literature, for copper species in well-defined materials. The parameters obtained experimentally for CuO bulk show an excellent agreement with those reported in the literature [10,44].

In an attempt to add more information on that subject, the Cu-$2p_{3/2}$ satellite peak has been analysed. It is known that for Cu-containing compounds, the existence of the characteristic satellite peak in the Cu-2p spectra is indicative of Cu^{2+} presence, since the d shells of Cu^0 and Cu^+ are filled and, therefore, cannot give rise to satellite peaks [5,45,46]. Thus, the relative proportion of Cu^{2+} species analysis can be approached by determining the ratio

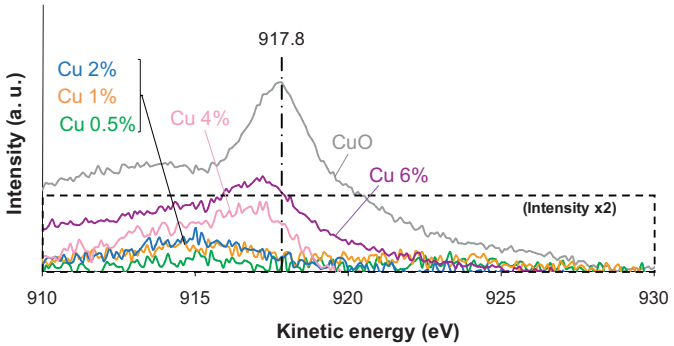

Fig. 4. Cu-L_3VV spectra of the samples (including CuO reference).

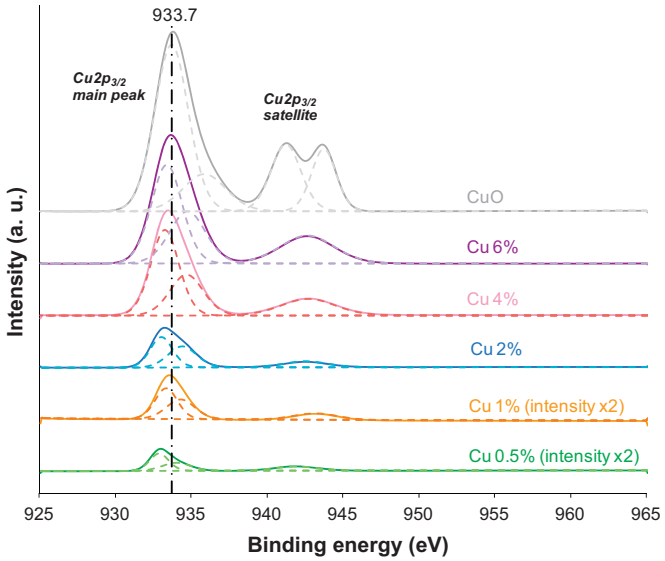

Fig. 5. Cu-$2p_{3/2}$ deconvoluted spectra for the samples, (fitted envelope and deconvoluted peaks).

Table 3
XPS parameters obtained from de Cu-$2p_{3/2}$ and Cu-L_3VV spectra.

	Cu$2p_{3/2}$ peak position (eV)	Auger parameter α' (eV)	A_{sat}/A_{mp}
CuO	933.7	1851.5	0.50
Cu 0.5%	932.9	1847.9	[a]
Cu 1%	933.4	1848.8	0.22
Cu 2%	933.1	1848.1	0.18
Cu 4%	933.3	1850.6	0.48
Cu 6%	933.4	1850.6	0.30
Cu 2%-re	933.2	1847.0	0.15

[a] Not determined due to the very low signal intensity.

between the satellite peak area (A_{sat}) to that of main Cu-$2p_{3/2}$ peak (A_{mp}), and by further comparison to values obtained with the bulk CuO reference sample ($A_{sat}/A_{mp} = 0.50$) [36,46].

The corresponding ratios for the copper-containing samples are listed on Table 3. It is observed that the results are far from 0.50 for the low copper content samples, and closer to 0.50 for Cu 4%

Table 4
Representative values of Cu-$2p_{3/2}$ binding energy (eV) and Cu-L_3VV Auger parameter (eV) reported in the literature for copper species in some well-defined materials [42,46].

	Cu-$2p_{3/2}$ binding energy (eV)	Auger parameter α' (eV)
Cu^{2+} (CuO)	933.8	1851.0
Cu^+ (Cu_2O)	932.5	1849.6
Cu^{2+} ions (exchanged in zeolites)	935.2	1849.5
Cu^+ ions (exchanged in zeolites)	933.8	1847.2

and Cu 6%, which also present similar values of main peak position and Auger parameter with regard to CuO. It is important to bear in mind that for those two samples, evidences of CuO phase were identified by XRD. Therefore, based on the whole experimental results, it should be underlined that copper is present mainly as a CuO-like phase for these two samples, although the presence of some Cu^{+} species cannot be discarded [8,11].

Conversely, the experimental evidences point out that the low values of A_{sat}/A_{mp} found for the rest of the samples suggest the coexistence of Cu^{2+}/Cu^{+} species during the XPS analysis. Due to possible photo reduction in the spectrometer, it is difficult to estimate the accurate degree of reduction of the copper species, but the calculations provide valuable information for catalysts comparison. Thus, according to the survey of literature, different hypothesis are compiled and underlined here in an attempt to explain these experimental results: (i) a better dispersion of copper yields to a higher photo reduction of copper, due to the X-ray irradiation during the XPS measurement [36] or (ii) due to strong support interfacial interaction, the Cu^{+} ions can be stabilised by interactions with the ceria-zirconia [10]. It should not be excluded the possible substitution of some cerium surface positions by some copper ions, although copper substitution into the fluorite structure was not confirmed by bulk techniques.

Finally, it should be noticed that the comparison of the binding energy (BE) and the Auger parameter (α') of the supported catalysts, obtained by the same synthesis procedure and the same precursors, provides some indirect and qualitative information about the dispersion degree of the supported phase, since these parameters are very sensitive to the dispersion degree of copper oxides. From 0.5 to 2% of copper loading, a high copper dispersion degree is suggested to take place, whereas for the highest copper loading, the existence of CuO bulk entities seems to be evident from the different techniques studied [39].

To conclude the characterisation part, we must also consider that the quantitative determination of dispersed CuO particles, by employing classical chemisorption techniques, is precluded in this type of samples due to the large reactivity of the support itself [27]. However, some qualitative information about the nature of copper species can be obtained from H_2-TPR patterns analysis.

3.3. H_2-TPR characterisation

H_2-TPR experiments have been carried out in order to investigate the reducibility of the catalysts, whose profiles are shown in Fig. 6(a) and (b). A single broad peak was found for the ceria-zirconia sample, starting at about 500 °C and centred at 608 °C. As all the samples were pre-treated in situ under O_2 at 500 °C to eliminate most of the surface contamination, it seems reasonable to deduce that the broad peak obtained corresponds to the reduction of Ce^{4+} to Ce^{3+} (Eq. (2)), because Zr^{4+} reduction occurs above 1000 °C [3,47]. Also, the presence of a single peak for this sample suggests that surface and bulk Ce^{4+} cations reduction occur concurrently due to the good bulk oxygen mobility allowed by the presence of Zr^{4+} cations in an appropriate ratio [3].

The reduction profile of pure CuO is characterised by a single peak at 350 °C. In contrast, a two-step reduction profile is observed for all the Cu-containing samples, with peak temperatures considerably lower than those of pure CuO and ceria-zirconia. This indicates the existence of a synergistic effect between copper and the mixed oxide which promotes improved reducibility [13,30,31,48–50].

In Fig. 6a, the reduction peaks observed from 160 to 300 °C should not be only attributed to copper reduction. Indeed, quantitative estimations reveal overall H_2 consumptions exceeding the amounts required for Cu^{2+} reduction, because considering the stoichiometry of Eq. (3), the H_2/CuO molar ratio should be 1.

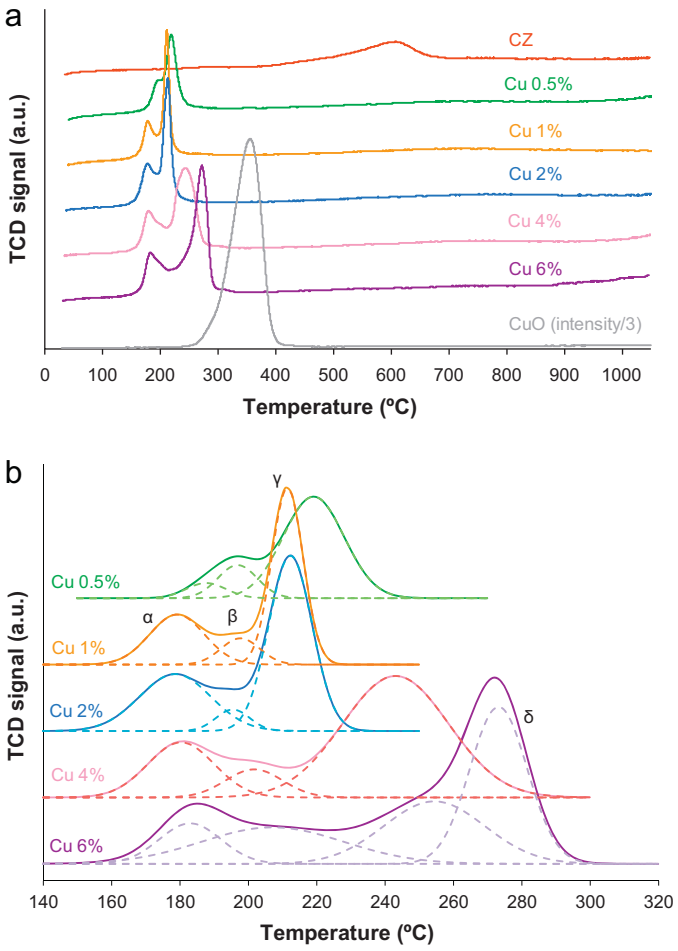

Fig. 6. (a) H_2-TPR profiles of the catalysts and the CuO reference sample and (b) deconvolution of the H_2-TPR profiles for the CuO/ceria-zirconia catalysts.

However, these experimental ratios, (expressed as H_2/CuO molar ratio obtained and listed in Table 5), underline that the H_2 consumptions are much higher than those necessary for the theoretical reduction of copper in the samples, suggesting that concomitant ceria reduction is also taking place, as agreed by several authors [13,31]. In addition, the contribution of hydrogen spillover on the support should not be excluded, according to Moretti et al., for Cu–Ce based materials [31].

$$2CeO_2 + H_2 \rightarrow Ce_2O_3 + H_2O \quad (2)$$

$$CuO + H_2 \rightarrow Cu + H_2O \quad (3)$$

The difference between the experimental and theoretical H_2 consumption is an estimation of the H_2 amount or "extra H_2" due to

Table 5
Quantitative analysis of H_2-TPR data for $CuO/Ce_{0.8}Zr_{0.2}O_2$ samples.

Catalyst	Theoretical H_2 consumption [a] (μmol/g)	Experimental H_2 consumption (μmol/g)	H_2/CuO molar ratio obtained
Cu 0.5%	79	851	10.8
Cu 1%	157	930	5.9
Cu 2%	315	1225	3.9
Cu 4%	630	1738	2.8
Cu 6%	944	2208	2.3
Cu 2%-re	315	1070	3.4

[a] Theoretical hydrogen consumption required to reduce the nominal amount of CuO, reaction (3).

ceria reduction (and potential spill over contributions). A quite linear relationship between the amount of H_2 due to ceria reduction and the copper content on samples has been found, (results represented on Fig. S5 of the Supporting Information), with the exception of Cu 0.5% whose estimation is similar to that of Cu 1%. This suggests that copper catalyses the reduction of cerium by H_2. Even though it is not easy to construct a direct correlation between the reduction characteristics of CuO-CeO_2 catalysts and their activity in oxidation reactions [51], this observation should be connected to the very similar NO to NO_2 oxidation curves shown by both samples, in spite of having different copper loadings, as we comment below. In fact, some qualitative relationships between H_2-TPR results and activity data can be established by copper-containing catalysts, in accordance with many authors [52].

In order to gain an insight into the reducibility behaviour of this series of samples, the deconvolution of the H_2-TPR curves has been performed and represented in Fig. 6b. The profiles of samples with low copper content consist of a combination of three broad contributions, denoted as α, β and γ. According to literature [53,54] and to our analysis, the attribution of the TPR contributions is as follows: the first peak (α) can be attributed to the reduction of highly dispersed copper oxide species, strongly interacting with ceria-zirconia [53]. The third peak (γ) is always quite intense and can be ascribed to the presence of CuO, with less interaction with the support, as well as the simultaneous Ce^{4+} reduction and H_2 spill over.

The Cu 0.5% profile is clearly different from those of Cu 1% and Cu 2%, beginning at higher temperature; but in spite of that, the Cu 0.5% catalyst is expected to present a high copper dispersion, as proven by XPS results and good catalytic activity results (shown below). In order to reconcile the experimental data obtained, it is important to pay attention to the second contribution (β). Some authors [55] assign this second contribution, appearing between the α and γ peaks, to the presence of isolated Cu^{2+} ions or highly dispersed clusters. According to Kundakovic et al. [55], when copper content is sufficiently low, copper is well-dispersed. This species is believed to be more difficult to reduce, thus appearing at higher temperatures than that of α peak. Therefore, the TPR profiles shown clearly reveal features related to structural/morphological differences in the CuO_x entities involved. For samples with 4 and 6% of copper, the contributions appear at higher temperatures, proving a lower reducibility due to a worse copper-support contact. Actually, the sample with the highest copper content presents a fourth contribution (δ), probably ascribed to bulk-like CuO particles, in accordance with the XRD analysis which revealed the tenorite CuO reflexions.

3.4. Catalytic oxidation of NO to NO_2

Fig. 7 shows the NO_2 percentage profiles obtained in catalytic tests performed without soot. A very low amount of copper on the catalyst improves the oxidation of NO to NO_2 with regard to the copper-free ceria-zirconia catalyst, decreasing the onset reaction temperature and shifting the maximum oxidation temperature towards lower values. In this sense, for ceria-zirconia, a maximum value of 26% NO_2 was found at 416 °C, while this value was 40% at 380 °C for the Cu 0.5% sample. These data are in accordance with previous results obtained in the CO-PROX reaction [12,13,26,27,31,38,50], where the performances of the CuO_x-CeO_2 and CuO_x-$Ce_xZr_{1-x}O_2$ catalysts appear to be improved by the presence of highly dispersed copper species on the ceria-based materials surfaces, favouring the formation of oxygen vacancies at the copper-ceria boundaries [8,11,12,27].

It is worthwhile to establish comparison among Cu 0.5%/Cu 1% samples and the CuO bulk sample, being the latter more active than the CZ support. The synergistic effect of the CuO/ceria-zirconia interfaces that promotes catalytic oxidation reactions, as reported

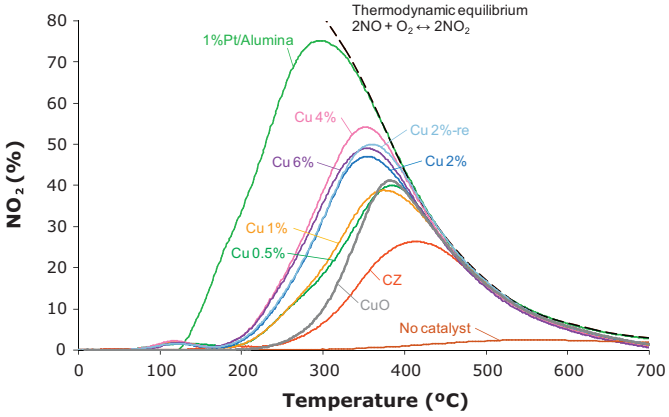

Fig. 7. NO_2 production profiles in TPR conditions for the catalysts.

by several authors [12,25], is clearly evidenced by the shift towards lower temperatures of the capacity to oxidise NO of the low copper content samples with regard to both CuO bulk and ceria-zirconia. However and as a consequence that CuO is also active for NO oxidation since 250 °C, the maximum activity reached by the lowest copper content samples is a little bit lower than that of CuO.

The samples with a 0.5 and 1% of copper showed quasi-identical oxidation curves, which could be consistent with their similar "extra-H_2" values estimated from H_2-TPR. On the other hand, higher NO_2 conversions are achieved by catalysts with copper contents between 2 and 6%, with minor differences among them. An optimum value was found for a 4% of copper loading. As the copper content increases, there is an enhancement in the copper surface enrichment (XPS), which affects the dispersion, the CuO_x/ceria-zirconia interfaces and cerium surface locations accessible to reaction gases, which are also catalytically active for the NO oxidation to NO_2. It is important to remind that bulk CuO is quite active for the NO to NO_2 oxidation reaction at high temperatures. The overall balance of all these factors seems to be very delicate, and as a consequence of this, the best behaviour is seen for Cu 4% sample. Even though, there are minor differences for the catalysts with copper content higher or equal than 2%.

Finally, the NO oxidation capacity of the copper/ceria-zirconia catalysts has been compared to that of a reference 1% Pt/alumina catalyst, and the NO_2 profile obtained with the noble metal catalyst has also been included in Fig. 7. As expected, the noble metal catalyst is much more active as NO oxidation catalyst, and the differences are more important at low temperatures, where thermodynamic restrictions do not exist. It has to be taken into account that soot combustion needs a minimum temperature of 250–300 °C to occur at an appreciable rate, and therefore, the NO_2 produced by the platinum catalyst below this threshold will not be really useful.

In order to compare the copper and platinum catalysts behaviour in the soot combustion reaction, isothermal experiments have been performed with selected catalysts at 400 °C.

3.5. Catalytic soot combustion

Firstly, soot combustion experiments under TPR conditions were carried out with the set of samples analysed in the previous section in order to select representative catalysts to perform the isothermal study. Fig. 8 illustrates the detail of the soot combustion curves (only low/medium temperatures and low values of conversion). It is interesting to note that the highest activity is shown by Cu 2% sample and the trends in activity exhibited by the samples are seen changed as the reaction temperature increases. Thus, for example, ceria-zirconia is the least active sample at the beginning of the reaction, but its behaviour is progressively improved until

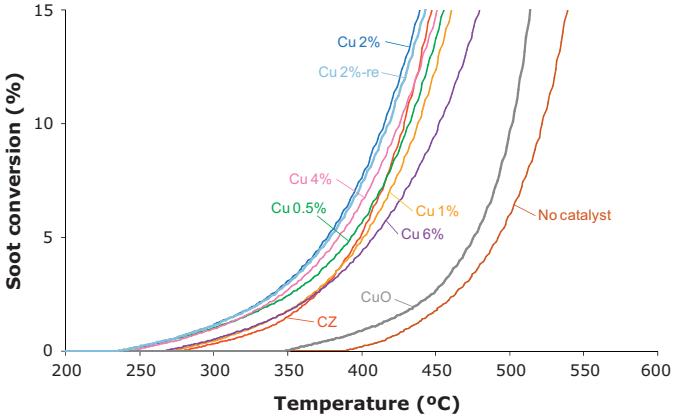

Fig. 8. Detail (only low and medium temperatures) of the soot combustion curves versus temperature for the ceria-containing catalysts studied. CuO sample and uncatalysed reaction are included for comparison purposes.

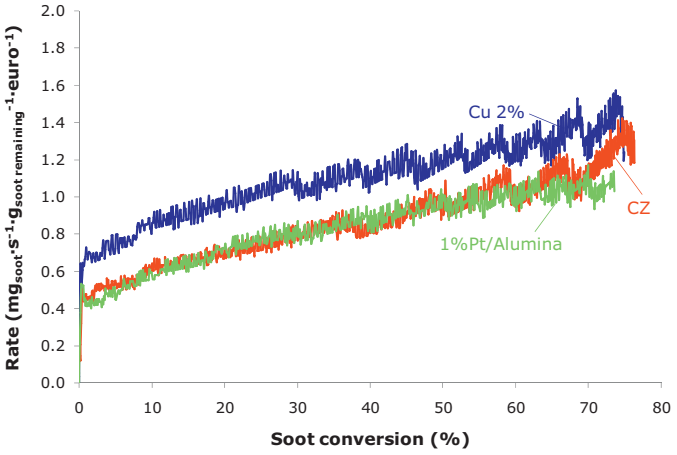

Fig. 10. Soot combustion rates, expressed per euro of catalyst cost, versus soot conversion in isothermal conditions (400 °C) for representative catalysts.

becoming the second sample in the activity order (just after Cu 2%). A reasonable hypothesis to explain these results is the relevance of the active oxygen assisted-soot combustion (becoming prevalent at high temperatures) besides the NO_2-assisted soot combustion, which is important to initiate the soot combustion process, as previously reported by the authors [2,56]. It is interesting to remind that the BET surface areas decrease progressively as the copper loading increases on the samples (from 96 to 57 m^2/g) and this fact diminishes the active oxygen transfer to the soot surface as the point of contacts among the soot surface and the catalyst particles play a key role under the loose contact mode. Therefore, it seems to be a compromise among a certain copper amount, which promotes an effective NO oxidation capacity at low temperatures and a minor loss in BET. The balance among these features yields Cu 2% as the optimum copper content for soot combustion under NO_x/O_2 in the range of temperatures considered.

From the results shown on Figs. 7 and 8, it is important to point out the similar catalytic performance between the samples Cu 2% and Cu 2%-re, which can be easily justified based on the similarity in their textural, structural and redox properties (see Tables 1–3 and Table 5). This confirms the reproducibility of the impregnation method to incorporate the copper onto the ceria-zirconia support.

Considering the results under temperature programmed conditions, Fig. 9 plots the isothermal soot oxidation rates at 400 °C against soot conversion for three representative catalysts: Cu 2%, the commercial 1% Pt/Al_2O_3 catalyst and the bare support, for comparative purposes. It has to be mentioned that the uncatalysed soot combustion rate is negligible in the experimental conditions of these experiments.

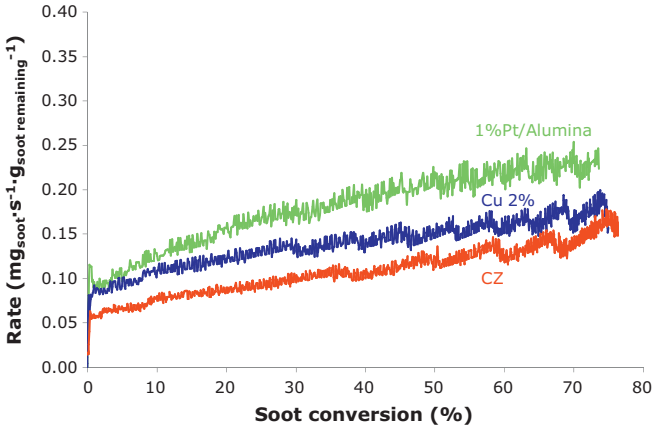

Fig. 9. Soot combustion rates versus soot conversion in isothermal conditions (400 °C) for representative catalysts.

Fig. 9 shows that 1% Pt/Al_2O_3 is the most active in terms of mass of catalyst, followed by Cu 2% and finally CZ, and this trend is consistent with the soot combustion profiles. However, the difference between the rate obtained with the 1% Pt/Al_2O_3 and the Cu 2% catalysts is always lower than 25%. This means that, from a practical point of view, the volume of a DPF loaded with a Cu 2% sample should be approximately 25% larger than that of a DPF loaded with 1% Pt/alumina (considering the same mass of catalyst per volume of DPF) to obtain similar soot combustion rates at 400 °C. The important conclusion is that this increase of the DPF volume can be assumed in a light-duty diesel vehicle.

In addition, if the soot combustion rates of Cu 2% and commercial 1%Pt/Al_2O_3 are compared in terms of price, the most efficient catalyst is Cu 2%, as shown in Fig. 10. The approximate price of each catalyst has been calculated only considering the price of the raw precursors [57] (see data in Table S1 from the Supporting Information) and the other variables involved in the manufacturing process have been ignored for simplicity. Obviously, these prices can fluctuate depending on the noble metals market, on the amount of catalyst prepared and so on, but this approximate estimation suggests that the copper/ceria-zirconia system could be a competitive substitute to the noble metal-based catalysts.

4. Conclusions

This research has been dedicated to the preparation, characterisation and study of the catalytic activity of CuO/ceria-zirconia catalysts, and the general conclusions that have been drawn are the following:

- BET surface areas and specific pore volumes of the catalysts decrease by increasing the copper content, due to the blocking of porosity.
- Experimental evidences about copper insertion into the structure of the ceria-zirconia support have not been found either by XRD or by Raman spectroscopy. According to XPS and H_2-TPR results, copper species are very well-dispersed onto ceria-zirconia, mainly at low copper loadings. Crystalline CuO entities have been identified only in samples with 4 and 6% of copper.
- The employed method (incipient wetness impregnation) yields reproducible samples, allowing the preparation of catalysts with very similar textural, structural and surface properties.
- Catalysts with copper drastically decrease the reduction temperature of CuO/ceria-zirconia samples, in H_2-TPR conditions, due

to the synergistic effect conferred by the copper–ceria interfacial interactions.

- The addition of a low copper content to the ceria-zirconia support dramatically accelerates the catalytic oxidation reaction of NO to NO_2, in relation to the support. An optimum value for the catalyst with 4% copper has been found.
- The soot combustion rate at 400 °C obtained with a copper/ceria-zirconia catalyst is somewhat lower than that of 1% Pt/Al_2O_3, but the difference is low enough to consider the use of copper/ceria-zirconia catalysts for DPFs regeneration in light-duty diesel vehicles, with the benefit of the lower price of a catalyst without noble metals.

Acknowledgements

The authors gratefully acknowledge the financial support of Generalitat Valenciana (Prometeo/2009/047 project), the Spanish Ministry of Economy and Competitiveness (CTQ2012-30703 project) and the UE (FEDER funding).

Appendix A. Supplementary data

Supplementary data associated with this article can be found, in the online version, at http://dx.doi.org/10.1016/j.apcatb.2014.01.018.

References

[1] A. Trovarelli, Catal. Ceria Relat. Mater. (2002).
[2] N. Guillén-Hurtado, A. Bueno-López, A. García-García, Appl. Catal. A: Gen. 437–438 (2012) 166–172.
[3] N. Guillén-Hurtado, A. Bueno-López, A. García-García, J. Mater. Sci. 47 (2012) 3204–3213.
[4] E. Aneggi, C. de Leitenburg, A. Trovarelli, Catal. Today 181 (2012) 108–115.
[5] L. Liu, Z. Yao, B. Liu, L. Dong, J. Catal. 275 (2010) 45–60.
[6] A.E. Nelson, K.H. Schulz, Appl. Surf. Sci. 210 (2003) 206–221.
[7] N. Guillén-Hurtado, I. Atribak, A. Bueno-López, A. García-García, J. Mol. Catal. A: Chem. 323 (2010) 52–58.
[8] A.P. Jia, G.S. Hu, L. Meng, Y.L. Xie, J.Q. Lu, M.F. Luo, J. Catal. 289 (2012) 199–209.
[9] F. Lin, X. Wu, D. Weng, Catal. Today 175 (2011) 124–132.
[10] A. Martínez-Arias, M. Fernández-García, J. Soria, J.C. Conesa, J. Catal. 182 (1999) 367–377.
[11] A. Martínez-Arias, A.B. Hungría, M. Fernández-García, J.C. Conesa, G. Munuera, J. Phys. Chem. B 108 (2004) 17983–17991.
[12] A. Martínez-Arias, D. Gamarra, M. Fernández-García, X.Q. Wang, J.C. Hanson, J.A. Rodriguez, J. Catal. 240 (2006) 1–7.
[13] A. Martínez-Arias, D. Gamarra, M. Fernández-García, A. Hornés, P. Bera, Z. Koppany, Z. Schay, Catal. Today 143 (2009) 211–217.
[14] X. Wu, Q. Liang, D. Weng, Z. Lu, Catal. Commun. 8 (2007) 2110–2114.
[15] Q. Liang, X. Wu, D. Weng, Z. Lu, Catal. Commun. 9 (2008) 202–206.
[16] P.S. Metkar, V. Balakotaiah, M.P. Harold, Catal. Today 184 (2012) 115–128.
[17] L. Olsson, H. Sjövall, R.J. Blint, Appl. Catal. B: Environ. 87 (2009) 200–210.
[18] L. Čapek, L. Vradman, P. Sazama, M. Herskowitz, B. Wichterlová, R. Zukerman, R. Brosius, J.A. Martens, Appl. Catal. B: Environ. 70 (2007) 53–57.
[19] F.E. López-Suárez, A. Bueno-López, M.J. Illán-Gómez, Appl. Catal. B: Environ. 84 (2008) 651–658.
[20] S. Suárez, S.M. Jung, P. Avila, P. Grange, J. Blanco, Catal. Today 75 (2002) 331–338.
[21] F.E. López-Suárez, A. Bueno-López, M.J. Illán-Gómez, A. Adamski, B. Ura, J. Trawczynski, Environ. Sci. Technol. 42 (2008) 7670–7675.
[22] S. Guerrero, G. Águila, P. Araya, Catal. Commun. 28 (2012) 183–190.
[23] A.P. Jia, S.Y. Jiang, J.Q. Lu, M.F. Luo, J. Phys. Chem. C 114 (2010) 21605–21610.
[24] Z.Y. Pu, X.S. Liu, A.P. Jia, Y.L. Xie, J.Q. Lu, M.F. Luo, J. Phys. Chem. C 112 (2008) 15045–15051.
[25] A. Martínez-Arias, M. Fernández-García, O. Gálvez, J.M. Coronado, J.A. Anderson, J.C. Conesa, J. Soria, G. Munuera, J. Catal. 195 (2000) 207–216.
[26] J.L. Ayastuy, A. Gurbani, M.P. González-Marcos, M.A. Gutiérrez-Ortiz, Int. J. Hydrogen Energy 37 (2012) 1993–2006.
[27] D. Gamarra, G. Munuera, A.B. Hungría, M. Fernández-García, J.C. Conesa, P.A. Midgley, X.Q. Wang, J.C. Hanson, J.A. Rodriguez, A. Martínez-Arias, J. Phys. Chem. C 111 (2007) 11026–11038.
[28] A. Hornés, A.B. Hungría, P. Bera, A.L. Cámara, M. Fernández-García, A. Martínez-Arias, L. Barrio, M. Estrella, G. Zhou, J.J. Fonseca, J.C. Hanson, J.A. Rodriguez, J. Am. Chem. Soc. 132 (2009) 34–35.
[29] K.A. Pokrovski, A.T. Bell, J. Catal. 241 (2006) 276–286.
[30] S.P. Wang, T.Y. Zhang, Y. Su, S.R. Wang, S.M. Zhang, B.L. Zhu, S.H. Wu, Catal. Lett. 121 (2008) 70–76.
[31] E. Moretti, L. Storaro, A. Talon, M. Lenarda, P. Riello, R. Frattini, M.d.V. Martínez de Yuso, A. Jiménez-López, E. Rodríguez-Castellón, F. Ternero, A. Caballero, J.P. Holgado, Appl. Catal. B: Environ. 102 (2011) 627–637.
[32] A. Bueno-López, I. Such-Basáñez, C. Salinas-Martinez de Lecea, J. Catal. 244 (2006) 102–112.
[33] M.R. Gallego, La difracción de los Rayos X (Alhambra ed.), 1982.
[34] F. Zhang, Q. Jin, S.W. Chan, J. Appl. Phys. 95 (2004) 4319–4326.
[35] A. Laachir, V. Perrichon, A. Badri, J. Lamotte, E. Catherine, J.C. Lavalley, J. El Fallah, L. Hilaire, F. Le Normand, E. Quéméré, G.N. Sauvion, O. Touret, J. Chem. Soc. Faraday Trans. 87 (1991) 1601–1609.
[36] U. Menon, H. Poelman, V. Bliznuk, V.V. Galvita, D. Poelman, G.B. Marin, J. Catal. 295 (2012) 91–103.
[37] W.J. Shan, W.J. Shen, C. Li, Chem. Mater. 15 (2003) 4761–4767.
[38] J.L. Ayastuy, A. Gurbani, M.P. González-Marcos, M.A. Gutiérrez-Ortiz, Int. J. Hydrogen Energy 35 (2010) 1232–1244.
[39] J.P. Espinós, J. Morales, A. Barranco, A. Caballero, J.P. Holgado, A.R. González-Elipe, J. Phys. Chem. 106 (2002) 6921–6929.
[40] I. Atribak, A. Bueno-Lopez, A. Garcia-Garcia, B. Azambre, Phys. Chem. Chem. Phys. 12 (2010) 13770–13779.
[41] G. Moretti, J. Electron Spectrosc. Relat. Phenom. 95 (1998) 95–144.
[42] A.F. Carley, M.K. Rajumon, M.W. Roberts, J. Solid State Chem. 106 (1993) 156–163.
[43] W. Grünert, N.W. Hayes, R.W. Joyner, E.S. Shpiro, M.R.H. Siddiqui, G.N. Baena, J. Phys. Chem. 98 (1994) 10832–10846.
[44] Perkin-Elmer, Handbook of X-ray Photoelectron Spectroscopy (1978).
[45] B. Skårman, T. Nakayama, D. Grandjean, R.E. Benfield, E. Olsson, K. Niihara, L.R. Wallenberg, Chem. Mater. 14 (2002) 3686–3699.
[46] B. Skårman, D. Grandjean, R.E. Benfield, A. Hinz, A. Andersson, L.R. Wallenberg, J. Catal. 211 (2002) 119–133.
[47] A. Łamacz, A. Krztoń, G. Djéga-Mariadassou, Catal. Today 176 (2011) 126–130.
[48] M.F. Luo, J.M. Ma, J.Q. Lu, Y.P. Song, Y.J. Wang, J. Catal. 246 (2007) 52–59.
[49] L. Ma, M.F. Luo, S.Y. Chen, Appl. Catal. A: Gen. 242 (2003) 151–159.
[50] P. Ratnasamy, D. Srinivas, C.V.V. Satyanarayana, P. Manikandan, R.S.S. Kumaran, M. Sachin, V.N. Shetti, J. Catal. 221 (2004) 455–465.
[51] G. Avgouropoulos, T. Ioannides, Appl. Catal. B: Environ. 67 (2006) 1–11.
[52] M.F. Luo, Y.J. Zhong, X.X. Yuan, X.M. Zheng, Appl. Catal. A: Gen. 162 (1997) 121–131.
[53] E. Moretti, L. Storaro, A. Talon, P. Riello, R. Frattini, M. Lenarda, Microporous Mesoporous Mater. 116 (2008) 575–580.
[54] H.B. Zou, X.F. Dong, W.M. Lin, Appl. Surf. Sci. 253 (2006) 2893–2898.
[55] L. Kundakovic, M. Flytzani-Stephanopoulos, Appl. Catal. A: Gen. 171 (1998) 13–29.
[56] I. Atribak, F.E. López-Suárez, A. Bueno-López, A. García-García, Catal. Today 176 (2011) 404–408.
[57] http://www.sigmaaldrich.com/spain.html.(accessed on October, 2013).